

GT2011-46543

EFFECT OF INLET SKEW ON HEAT/MASS TRANSFER FROM A SIMULATED TURBINE BLADE

Kalyanjit Ghosh* and R. J. Goldstein†

Heat Transfer Laboratory
Department of Mechanical Engineering
University of Minnesota, Minneapolis, MN 55455
Tel: 612-625-5552, Fax: 612-625-3434
Email: kalmech@me.umn.edu, rjg@me.umn.edu

ABSTRACT

Heat (mass) transfer experiments are conducted to study the effect of an inlet skew on a simulated gas-turbine blade placed in a linear cascade. The inlet skew simulates the relative motion between rotor and stator endwalls in a single turbine stage. The transverse motion of a belt, placed parallel to and upstream of the turbine cascade, generates the inlet skew. With the freestream velocity constant at approximately 16 m/sec, which results in a Reynolds number (based on the blade chord length of 0.184 m) of 1.8×10^5 , a parametric study was conducted for three belt-to-freestream velocity ratios. The distribution of the Sherwood number on the suction surface of the blade shows that the inlet skew intensifies the generation of the horseshoe vortex close to the endwall region. This is associated with the development of a stronger passage vortex for a higher velocity ratio, which causes an earlier transition to turbulence. Corresponding higher mass transfer coefficients are measured between the mid-height of the blade and the endwall, at a mid-chord downstream location. However, a negligible variation in transport properties is measured above the two-dimensional region of the blade at the higher velocity ratios. In contrast, the inlet skew has a negligible effect on the distribution of the Sherwood number on the entire pressure surface of the blade. This is mainly because the skew is directed along the passage vortex, which is from the pressure surface of the airfoil to the suction surface of the adjacent airfoil.

Keywords: mass transfer, heat/mass transfer analogy, naphthalene sublimation, inlet skew, simulated blade

NOMENCLATURE

C chord length of blade (= 18.4 cm)
 C_{ax} axial chord length of blade (= 13.0 cm)
 c_1 absolute velocity, Fig. 1(b)
 D diffusion coefficient of naphthalene in air
 H height of test section
 h_m mass transfer coefficient
 I/E inlet/exit ratio
 n_{min} minimum boundary layer thickness in normal direction
 P pitch length of blades (= 13.8 cm)
 r velocity ratio (= u_w/u_{in})
 Re_{in} inlet Reynolds number based on chord length (= $\rho u_{in} C / \mu$)
 S_p, S_s curvilinear coordinates along pressure, suction surfaces
 Sh Sherwood number (= $h_m C / D$)
 Tu turbulence intensity
 u_{in} freestream velocity
 u_s belt velocity
 u_1 rotor velocity, Fig. 1(b)
 w_1 relative velocity, Fig. 1(b)
 x coordinate in the streamwise direction, Fig. 2
 x_b coordinate along endwall, Fig. 3(a)
 y, y_b vertical direction
 z_b coordinate transverse to endwall, Fig. 3(a)
 z cross-stream coordinate, Fig. 2

*Presently at GE Global Research, Bangalore, India.

†Address all correspondence to this author.

Greek Symbols

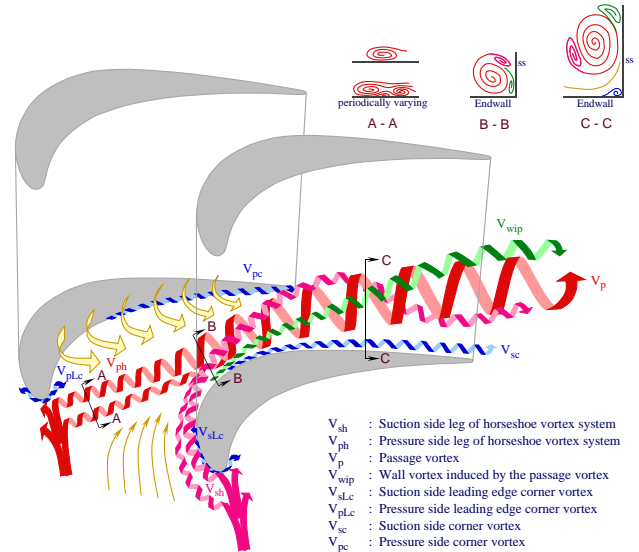
- β_1 blade inlet angle ($= 35^\circ$)
- β_2 blade outlet angle ($= -72.49^\circ$)
- δy sublimation depth
- δt wind tunnel run time
- Δ uncertainty parameter
- ρ_s density of solid naphthalene
- $\rho_{v,w}$ naphthalene vapor density on the surface
- $\rho_{v,\infty}$ naphthalene vapor density in freestream

INTRODUCTION

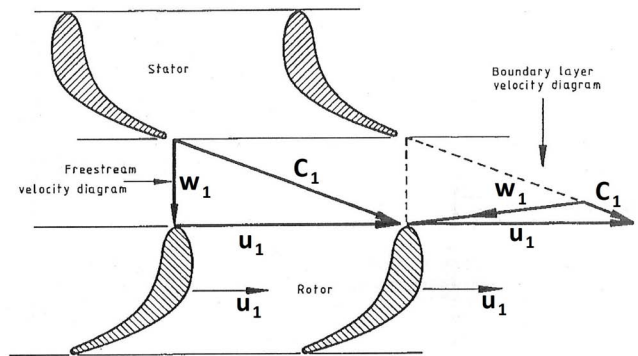
Secondary flows are generated in a turbine cascade due to the cumulative effect of: *i*) turning of the inlet vortices through the blade passages and *ii*) the presence of the end wall. A schematic of the horseshoe and passage vortex systems is shown in Fig. 1(a) [1]. In this stationary cascade, the pressure leg of the horseshoe vortex (V_{ph}) is directed towards the suction surface of the adjacent airfoil due to a strong passage pressure gradient. The suction side leg (V_{sh}) is pulled away from the end wall by the passage vortex and becomes wrapped around it. It (V_{sh}) remains close to the suction surface as it grows downstream. A strong vortex system, V_{wip} (Fig. 1(a)), is also observed close to the suction surface, which stays above the passage vortex and counterrotates against it. The losses associated with the secondary flows form a major proportion of the total losses in the cascade. A single turbine ‘stage’ consists of a row of stationary airfoils called the ‘vanes’, which pre-turns the flow as it spins the downstream row of ‘blades’. An actual turbine consists of a number of these ‘stages’ to increase the total power output. This relative motion between the vanes and the blades greatly affects the overall losses in the cascade. However, experimental heat (mass) transfer studies have mostly been performed in a stationary cascade, due to the inherent measurement challenges associated with moving parts, leading to results that may not be entirely applicable to gas-turbines.

A moving belt was used to generate a skewed boundary layer upstream of an impulse turbine cascade by Carrick [2]. Flow-field measurements using pressure probes showed a considerable increase in the secondary losses with inlet skew. Bindon [3] determined that a strong streamwise vorticity is produced in the same direction as the passage vortex and is fed by the transverse blade-to-blade pressure gradient. Fig. 1(b), which shows the boundary layer velocity diagram over the blade leading edge endwall region, indicates that the flow has a significant tangential component in the frame of reference of the rotor due to the no-slip boundary condition at the endwall. In a subsequent study [4], Bindon observed that the passage vortex was lifted away from the endwall due to skewing. This was attributed to the endwall cross-flows being radially directed as they strike and rise on the suction surface. However, the overall losses were reduced for this cas-

cade. This result was surprising, and as pointed out in a later study [5], the losses were affected due to the removal of the inlet velocity boundary layer through a slot immediately upstream of the cascade. Walsh and Gregory-Smith [6] observed that the inlet skewness caused a more rapid development of the passage vortex than without a skew. In addition, the pressure-side leg of the horseshoe vortex crossed the endwall earlier, with more intense cross flows behind it. In a later study [5], it was determined that the effect of the skewness on the losses was more important than the effect of the thickness of the inlet boundary layer.



(a) Schematic of horseshoe and passage vortex system [1]



(b) Velocity boundary layer over the end wall region (modified from [3])

Figure 1. Secondary flows in a cascade and velocity boundary near the end wall

In addition to cases involving moving endwalls, a number of studies have been performed on the interaction of passing wakes on a turbine cascade. Dullenkopf et al. [7] found negligible effects of the wake size on the distribution of the mean heat transfer

coefficient on the blade. Boletis and Sieverding [8] studied the three-dimensional flow field through a turbine stator preceded by a full stage. They observed that the overall shape of the inlet skew does not resemble those generated in isolated cascades by rotating the upstream endwalls. Zhang and Han [9] noted that the effect of the freestream turbulence on the blade heat transfer diminishes with an increase in the wake passing frequency. Chaluvadi et al. [10] studied the flowfield within the blade rows of a single-stage axial turbine using five-hole pneumatic and three-axis hot wire probes. Flow visualization studies were conducted using the smoke-wire technique. It was observed that the pressure side leg of the vane passage vortex was entrained into the rotor passage vortex. Schlienger et al. [11] studied the interaction between the vane wake, the turbine blades, and the secondary flow vortices in the blade passages. Schobeiri et al. [12, 13] observed a periodic expansion and contraction of the separation region on the suction surface of a blade with the passage of wake flow. More recently, mean and unsteady heat transfer measurements using thin film gauges were conducted by Allan et al. [14] on the midheight streamline of rotor blades.

The objective of the present study is to examine the effect of a skewed turbulent boundary layer on the heat (mass) transfer from a simulated gas turbine blade. A rubber belt, translating parallel to and upstream of the cascade row, generates the inlet skew. The distribution of the heat (mass) transfer coefficient is measured using the naphthalene sublimation technique based the heat-mass transfer analogy. A parametric study is conducted with the inlet freestream velocity, $u_{in} = 16 \text{ m/sec}$, and the belt velocity $u_w = 0, 8 \text{ and } 10 \text{ m/sec}$. The detailed spatial resolution and accuracy of the measurements make them appropriate for an increased fundamental understanding and for assessments of computational models.

EXPERIMENTAL APPARATUS

A blower wind tunnel, previously used by Olson [15] is used in this study. Room air enters the contraction region through a transition duct followed by flow straighteners and dampening screens. The contraction region has an area ratio of 6.25:1. Subsequently, the flow is tripped at the inlet of the test-section with a wire of diameter 1.4 mm to ensure turbulent flow conditions. The plexiglass test-section is a square-shaped duct $45.7 \times 45.7 \text{ cm}^2$ in cross-section.

The moving endwall, previously used by Srinivasan and Goldstein [16] and Ghosh and Goldstein [17], is placed parallel to and upstream of the linear cascade. It consists of a rubber belt passing over a set of three rollers, one of which is driven by an electric motor. The motor speed is controlled using a Altivar-ATV controller and the corresponding belt speed is measured using a handheld digital tachometer (reading accuracy of $\pm 0.06\%$ and resolution of 0.01 in the range $0.02 - 999.9 \text{ m/min}$). Fig. 2 shows the location of the moving belt upstream of the blade cascade in the wind tunnel. Vibration/flutter of the belt has been

previously measured using a high speed camera and is negligible compared to the boundary layer thickness of the inlet flow.

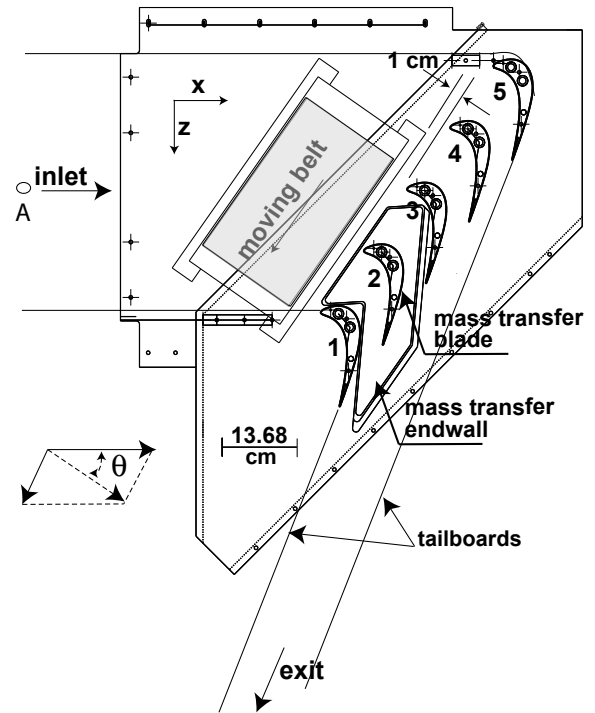


Figure 2. Position of belt upstream of cascade

The stationary cascade consists of a set of five aluminum airfoils, which are large-scale models of a first stage rotor blade. It is characterized by a high aspect ratio (span/actual chord) of 2.48, allowing a clear separation of the endwall effects on flow through the cascade. The blade geometry, as shown in Fig. 3(a), turns the flow through an angle of 107.5 deg . Additional details of the cascade are listed in Table 1. Flow entering the blade row is negatively skewed by the upstream moving belt (from the suction to the pressure surface). Downstream of the moving belt and the cascade, the flow exits the wind-tunnel guided by a pair of tailboards. Mass transfer experiments are conducted on a simulated blade made of aluminum, as shown in Fig. 3(b), positioned at location 2 (Fig. 2). The active surface on the blade, coated with naphthalene, forms approximately 97% of the total height of the blade. The co-ordinate system in the frame of reference of the inlet flow is denoted by x, y, z (Fig. 2) and in the frame of reference of the endwall is given by x_b, y_b, z_b (Fig. 3(a)). Wetted distances along the suction and the pressure surfaces are denoted

by S_s and S_p , respectively. Subsequently, S_s/C varies from 0 (leading edge) to 1.38 (trailing edge) and $0 \leq S_p/C \leq 1.07$.

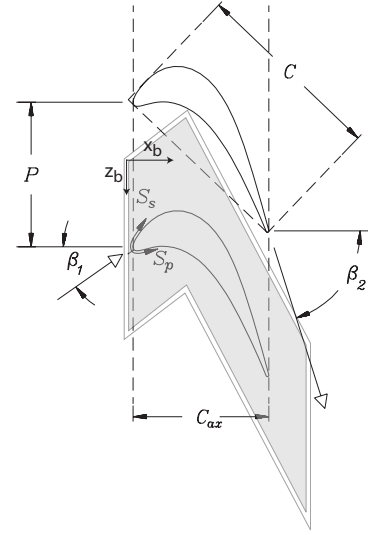
Table 1. Blade cascade geometry parameters

Item	
Chord length of blade - C	184.15 mm
Axial chord of blade - C_{ax}	129.64 mm
Blade pitch of cascade - P	138.11 mm
Height (Span) of Cascade - H	457.2 mm
Width of Cascade Inlet - W	457.2 mm
Number of blades	5
Axial Chord to Chord ratio - C_{ax}/C	0.704
Solidity (Pitch/Chord) - C/P	1.333
Aspect ratio (Span/Chord) - H/C	2.483
Blade inlet angle - β_1	35°
Blade outlet angle - β_2	-72.49°
Inlet/Exit area ratio of cascade (I/E)	2.72
Inlet contraction area ratio	6.25
Height of mass transfer blade	196.5 mm
Height of active coated surface	190.5 mm
Maximum Surface distance (S_s/C)	1.3813
Maximum Surface distance (S_p/C)	1.0685

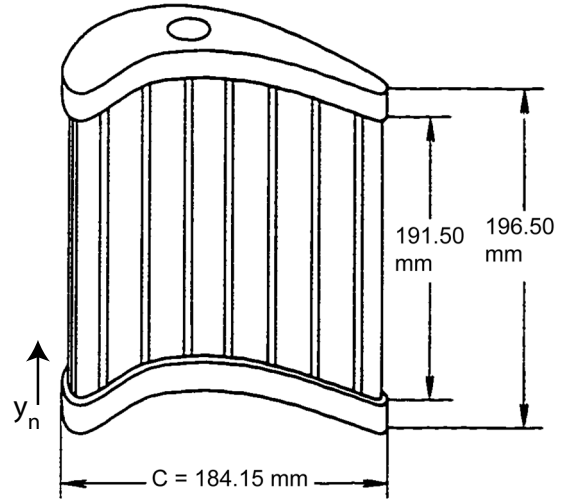
At an approximately constant inlet velocity $u_{in} = 16 \text{ m/sec}$, the axial velocity is given by $u_{ax} = u_{in} \cos \beta_1$, where β_1 is the blade inlet angle. Subsequently, belt speeds of $u_w = 0, 8$ and 10 m/sec gives belt-to-axial velocity ratios of ($r = u_w/u_{ax}$) equal to 0, 0.61 and 0.76 respectively. This corresponds to nominal values of $r \sim O(1)$, which is encountered in the actual operation of a gas turbine engine. The average exit Reynolds number ($Re_{ex} = \frac{\rho \cdot I/E \cdot u_{in} \cdot C}{\mu}$) is approximately equal to 5.22×10^5 , where AR is the aspect ratio ($=2.72$) and C is the chord length ($= 184 \text{ mm}$). It should be noted that the freestream velocity is selected to match the preliminary results with two previous studies in the same cascade (Han [18], $Re_{ex} = 4.5 \times 10^5$; Papa [19], $Re_{ex} = 6 \times 10^5$).

MEASUREMENT PROCEDURE

The volumetric flow through the cascade is balanced using a hollow aluminum blade (placed in location of Blade 2, Fig. 2),



(a) Top view



(b) Side view

Figure 3. Mass transfer blade geometry

with static pressure taps along the suction and the pressure surfaces. The distribution of the static pressure coefficient over the blade surface is shown in Fig. 4 along with the inviscid flow solution, obtained previously using the commercial software FLUENT [19]. The tailboards are adjusted to vary the flow through the blade passages to obtain the closest approximation to the numerical solution. Subsequently, the static pressure blade is replaced by a solid blade during the actual experiment.

Heat Mass Transfer Analogy

The heat/mass transfer analogy is based on the idea that in incompressible constant property flows, temperature and concen-

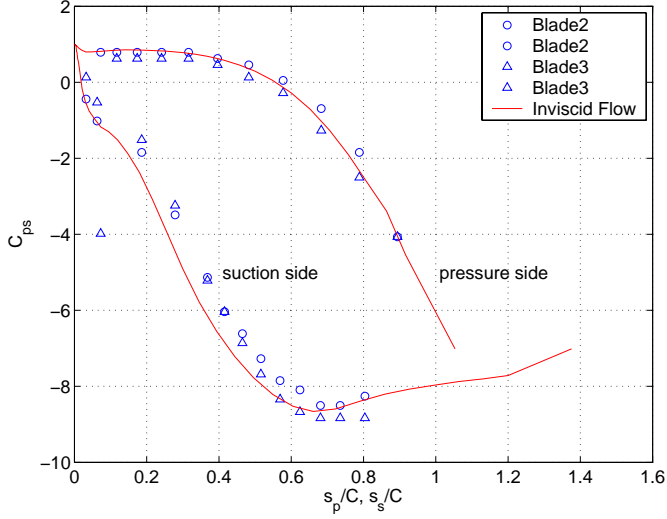


Figure 4. Static pressure distribution on the surface of the blade

tration (non-reacting species) are passive scalars and have no bearing on the fluid dynamics [20, 21]. The transport equations for the non-dimensional thermal and mass concentration in a turbulent boundary layer are given by

$$\frac{D\theta}{Dt} = \frac{1}{Re_x Pr} \frac{\partial}{\partial \hat{x}_i} \left[\left(1 + \frac{\varepsilon Pr}{\nu Pr_t} \right) \frac{\partial \theta}{\partial \hat{x}_i} \right] \quad \text{heat transfer} \quad (1a)$$

$$\frac{D\Phi}{Dt} = \frac{1}{Re_x Sc} \frac{\partial}{\partial \hat{x}_i} \left[\left(1 + \frac{\varepsilon Sc}{\nu Sc_t} \right) \frac{\partial \Phi}{\partial \hat{x}_i} \right] \quad \text{mass transfer} \quad (1b)$$

Goldstein and Cho [22] have provided a detailed review of the mass transfer analogy and the naphthalene sublimation technique. A mass transfer study is more suited for complex flows as compared to heat transfer experiments, as errors associated with wall conduction and radiation are negligible. However, as pointed out by Eckert et al. [23], the boundary conditions should be equivalent for the analogy to be valid. For the heat/mass transfer analogy considered in this study, the similarity conditions are

Heat Transfer: $Re_x, Pr, T_w = \text{constant}$, model shape

Mass Transfer: $Re_x, Sc, c_w = \text{constant}$, model shape

Naphthalene Sublimation Technique

The naphthalene sublimation technique is used to determine the distribution of the local mass transfer coefficients on the simulated blade. The surface is coated with naphthalene using a casting process and is scanned using a LVDT (linear variable differential transformer) probe. Subsequently, it is placed in the wind-tunnel for the duration of the experiment. A post-run LVDT measurement of the surface is conducted and the sublimation depth during the run is obtained from the difference in these measurements. Finally, the local mass transfer coefficients on the surface of the plate are determined from

$$h_m = \frac{\dot{m}}{\rho_{v,w} - \rho_{v,\infty}} = \frac{\rho_s \delta y / \delta t}{\rho_{v,w}} \quad (2)$$

Subsequently, the mass transfer coefficient Sh is given by

$$Sh = \frac{h_m \cdot C}{D} \quad (3)$$

Uncertainty Analysis

The uncertainty in the mass transfer Sherwood number (ΔSh) is calculated using the methods described by Kline and McClintock [24] at a 95% confidence level. As shown in Eqn. 4, ΔSh depends on the individual uncertainties of the blade chord length (ΔC), mass transfer coefficient (Δh_m) and the diffusion coefficient (ΔD).

$$\frac{\Delta Sh}{Sh} = \left[\left(\frac{\Delta h_m}{h_m} \right)^2 + \left(\frac{\Delta C}{C} \right)^2 + \left(\frac{\Delta D}{D} \right)^2 \right]^{1/2} \quad (4)$$

Here, ΔC is negligible compared to the others, as the chord length is fixed during the experiments. The uncertainty in the mass transfer coefficient ($h_m = \frac{\rho_s \delta y}{(P_{v,w}/RT_w) \delta t}$) is calculated from the individual uncertainties of the following quantities:

$$\Delta \rho_s / \rho_s = 1.10\% \quad ([22])$$

$$\Delta \delta y / \delta y = 1.20\% \quad (\text{calibration, noise, reading and free convection errors})$$

$$\Delta T_w / T_w = 0.15\% \quad (\text{reading uncertainty})$$

$$\Delta \delta t / \delta t = 0.42\% \quad (\text{reading error})$$

$$\Delta P_{v,w} / P_{v,w} = 3.77\% \quad ([22])$$

The uncertainty in the diffusion coefficient (ΔD) is estimated from the uncertainties claimed by Cho [25] and Chen and Wung [26] to be 4.1% [22]. Subsequently, the total uncertainty in Sh is approximately equal to 6%. It should be noted that the precision error amounts to only 1.2% whereas the bias error (from uncertainties in the properties of naphthalene) constitutes the major portion of the total error.

The surface profile of the blade is measured using a four-axis measurement table as shown in Fig. 5. The LVDT probe is mounted on a setup housing three unislides, which moves it along the x_b, y_b, z_b directions. The blade is fixed on a rotary table which rotates it in the θ direction, such that the probe is normal to the surface of blade at all positions. The system is driven by stepper motors connected to a PC terminal through IEEE-488 GPIB buses. The LVDT probe is calibrated using a set of precision gage blocks to obtain a linear displacement vs. voltage response (1 V corresponds to a displacement of 52.42 μm). Results from a mock sublimation test with a square aluminum

plate (non-sublimating or inactive surface) shows that the probe gives a mean displacement of 24 nm with a standard deviation of 177 nm . With the average sublimation depth during an actual run being approximately $60 \mu\text{m}$, the system has adequate resolution to measure the surface profile accurately. The actual depth change in an experiment is determined after correcting for the natural convection loss during the time the naphthalene surface is exposed to ambient conditions.

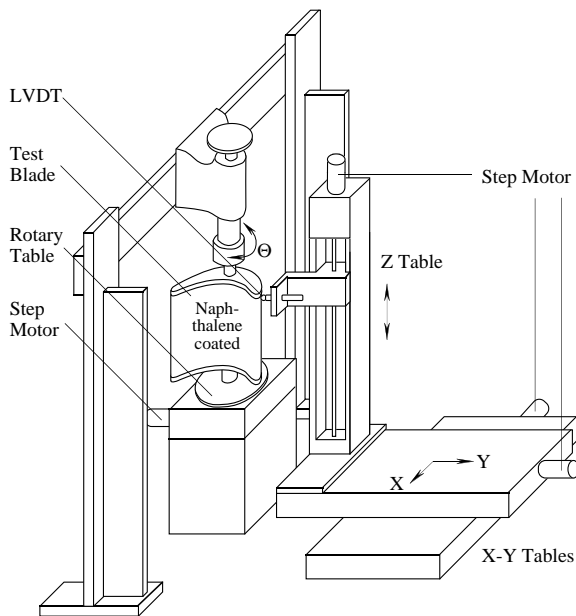


Figure 5. Mass transfer measurement table

Numerical Simulation

A numerical simulation using FLUENT is conducted to compare with the experimental data. The top-view of the 3-D computational domain, meshed in GAMBIT, is shown in Fig. 6. The two lateral sides of the geometry are obtained by translating the blade camberline by half the blade pitch along the $+z_b$ and $-z_b$ directions. The height of the entire domain is equal to half the wind-tunnel height. The bottom surface is meshed using the ‘Quad-Pave’ meshing scheme and the volume mesh is generated using a ‘Cooper’ meshing scheme. A boundary layer is attached to the blade surface as well as to the entire bottom surface to refine the mesh in the vicinity of the wall. Boundary conditions applied to the geometry are shown in Fig. 6. A SYMMETRY condition is applied to the top surface of the 3 volumes formed by area.1, area.2 and area.3. The moving belt is simulated by area.2, and its trailing edge lies 4.3 cm ($0.33C_{ax}$) upstream of the leading edge of the blade. The inlet and outlet of the domain extends to $0.33C_{ax}$ upstream of the leading edge of the belt and C_{ax} downstream of the trailing edge of blade, respectively.

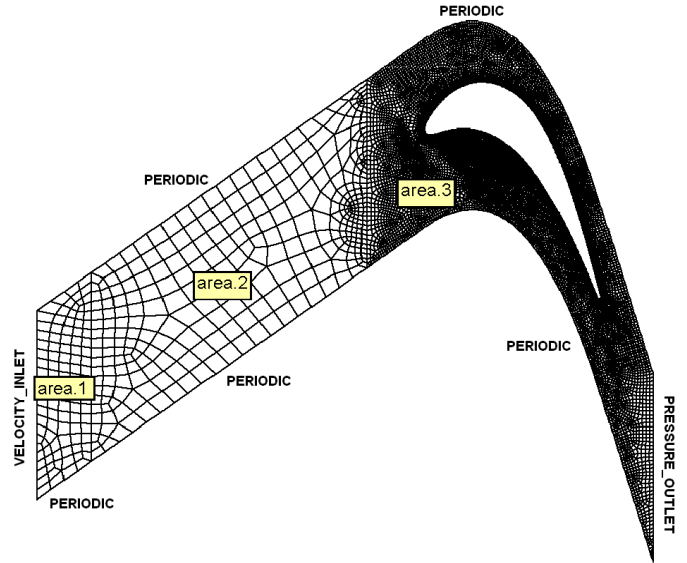


Figure 6. Mesh Geometry in Gambit

A WALL boundary condition is applied to the entire bottom surface. The SST $k - \omega$ turbulence model, originally proposed by Menter [27], is used to perform the numerical simulation in this study. In this model, the $k - \omega$ model is used in the near-wall region and it changes into a $k - \epsilon$ model away from the wall. This model has previously been used by various researchers to investigate flow and heat transfer in linear cascades [28,29,30,31,32]. Profiles of the velocity, kinetic energy (k) and specific dissipation rate (ω) are specified at the inlet. These profiles are obtained from a separate 2-D FLUENT simulation, hereafter referred to as the *inlet simulation*. The *inlet simulation* models the development of a turbulent boundary layer from an uniform velocity profile in a rectangular domain (length = 736 mm) and is used to compare the velocity results from a separate experimental study [17]. The length of this domain is equivalent to distance of the virtual origin of the turbulent boundary layer from the leading edge of the blade. The virtual origin is determined a priori from velocity profiles (measured using a single hot-wire) at various streamwise locations. Grid independency is tested by comparing the results between the meshes listed in Table 2. Mesh 1 is eventually used to compare with the experimental study involving the stationary and the moving belt (inlet skew).

RESULTS AND DISCUSSION

In this section, a comparison of the experimental and CFD results are presented.

Suction Surface

The experimental distribution of the Sherwood number with the stationary belt (base case) is shown in Fig. 7(a). As noted before, the trailing edge of the blade is located at $S_s/C = 1.38$. A

Table 2. Mesh conditions

	Mesh 1	Mesh 2	Mesh 3	Mesh 4
$n_{min}(blade)$	first 0.05 growth 1.1	first 0.05 growth 1.2	first 0.05 growth 1.1	first 0.05 growth 1.1
area.1 (mesh faces)	105	105	105	105
area.2 (mesh faces)	353	194	302	353
area.3 (mesh faces)	19937	18512	20196	19937
volume.1 (mesh volumes)	9450	6300	8400	15750
volume.2 (mesh volumes)	31770	11640	24160	52950
volume.3 (mesh volumes)	1794330	1110720	1615680	2990550

‘first 0.05 growth 1.1’ denotes a boundary layer mesh with the first thickness equal to 0.05 mm and a growth ratio of 1.1

triangular region of high Sh is observed near the endwall corresponding to the lifting of the suction side leg of the horseshoe vortex (V_{sh} , Fig. 1(a)). This vortex is initiated close to the end-wall corner at about one-third the chord length and weakens as it is carried downstream by the passage vortex (V_p). At the leading edge ($S_s/C = 0$), high values of Sh are observed due to stagnation of the incoming flow. It decreases rapidly as a velocity boundary layer develops in the streamwise direction. A local laminar wedge-flow similarity solution [33] for $Pr = Sc = 2.28$ ($Re_{ex} = 1.76 \times 10^5$), at $y_b/C = 0.040$ and $y_b/C = 0.509$ is also shown for comparison (Fig. 8). The similarity solution is obtained as follows: velocity profile from the potential flow theory is used to define a local similarity variable, m , which is subsequently used to solve the local laminar wedge-flow similarity equations of momentum, heat, and mass transfer. The approximate analytical method is described by Sparrow et al. [34]. An excellent agreement with the laminar flow solution, especially prominent in the two-dimensional region ($y_b/C > 0.5$), is observed from these plots. However, at $y_b/C = 0.04$, the agreement is observed only till $S_s/C \approx 0.3$, which is due to the 3d region on the blade suction surface.

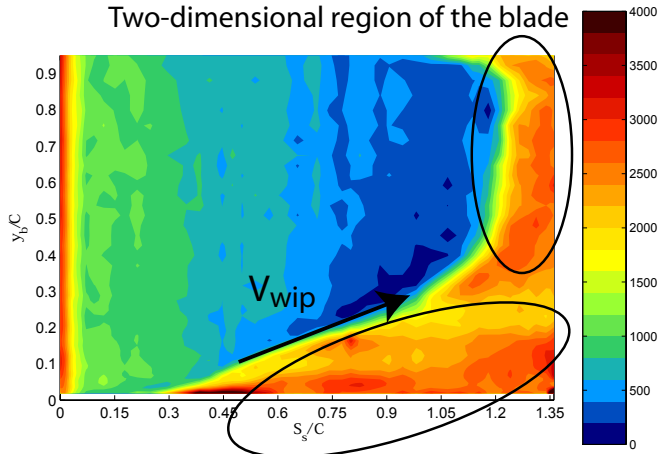
Downstream of the leading edge, an increase in Sh is observed near the endwall ($y_b/C = 0.019$) beginning at $S_s/C = 0.2$ with a peak value lying between $0.4 < S_s/C < 0.45$. This region of high Sh has roughly a triangular shape as it grows on the blade surface (Fig. 7(a)). This peak coincides with the formation of the wall induced vortex, V_{wip} , which lies above the passage vortex (Fig. 1(a)). It is convected downstream along with V_p , and gradually reduces in strength. This new vortex has been previously shown by a number of studies [33,35]. Between $0.019 < y_b/C < 0.5$, this peak gradually subsides as the suction side leg moves away from the blade surface. Correspondingly, the location of minimum Sh moves towards the trailing edge.

In the two-dimensional region ($y_b/C > 0.5$), the minimum mass transfer region is observed between $0.95 < S_s/C < 1.05$, which corresponds to the laminar separation of the flow at these locations. Downstream of this minimum, transition and turbulent

reattachment is observed at approximately $S_s/C = 1.2$. It should be noted that most of the blade surface experiences a laminar boundary flow and therefore, the power index of $n = 1/3$ can be used in $Nu/Sh = (Pr/Sc)^n$ to determine heat transfer Nusselt numbers from the mass transfer Sherwood numbers. Contour plots of the variation of Sh at the higher velocity ratios are shown in Figs. 7(b) and 7(c).

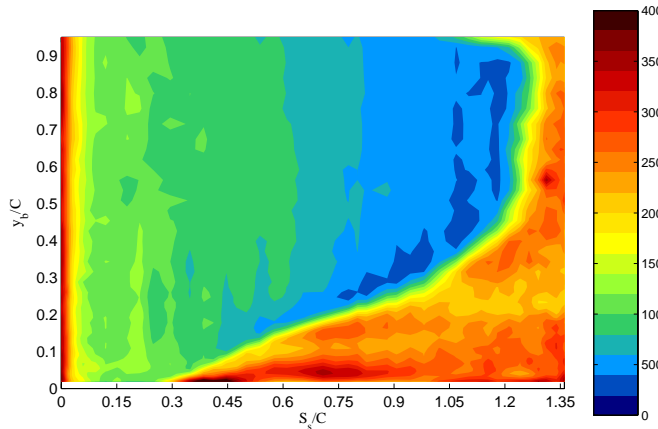
A detailed comparison of Sh at various y_b/C locations for different belt velocities is shown in Fig. 8. The developing secondary flow region near the endwall surface moves upstream with the belt motion. At $y_b/C = 0.019$, the wall induced vortex (V_{wip}) crosses the suction surface at $S_s/C = 0.40$ for $u_w = 8, 10$ m/sec compared to $S_s/C = 0.45$ for the base case ($u_w = 0$ m/sec). Downstream of $S_s/C = 0.6$, a negligible variation in Sh between the three cases is observed, which is mainly due to the development of a high turbulent region. Higher Sh corresponding to the higher belt speed is observed between $0.4 < S_s/C < 0.6$ until $y_b/C < 0.1$. Beyond $y_b/C > 0.1$ and until $y_b/C \approx 0.3$, an earlier transition to turbulence (corresponding to the triangular region in Fig. 7(a)) is observed with the moving belt. This corresponds to the passage vortex being lifted and strengthened by the inlet skew, as determined by previous studies [4, 6, 36]. It also appears that in the two-dimensional portion of the blade ($y_b/C > 0.5$), the location of the transition and reattachment regions is delayed with the belt motion. The numerical solution using FLUENT predicts a similar ‘earlier’ transition to turbulence in the triangular region of the blade ($y_b/C < 0.35$, Fig. 9). In the two-dimensional region, no difference in the location of the laminar separation is predicted at a higher belt-velocity compared to the stationary case. However, the disagreement of the CFD with the experimental results in predicting the transition to turbulence in the 2D region ($y_b/C > 0.4$) is evident. This is primarily due to the inability of the present turbulence models in predicting the near wall region in the flow which is highly 3D. Overall, the comparison between the numerical and the experimental results is quite good.

Pressure Surface

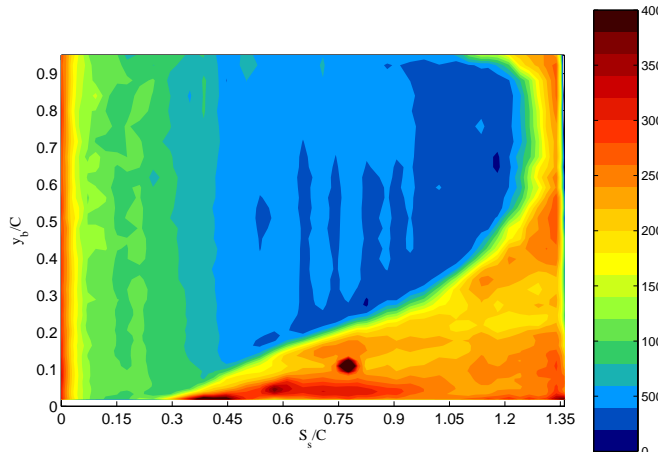


Three-dimensional region of the blade

(a) Stationary belt



(b) $u_w = 8 \text{ m/sec}$



(c) $u_w = 10 \text{ m/sec}$

Figure 7. Experimental distribution of Sh on suction surface

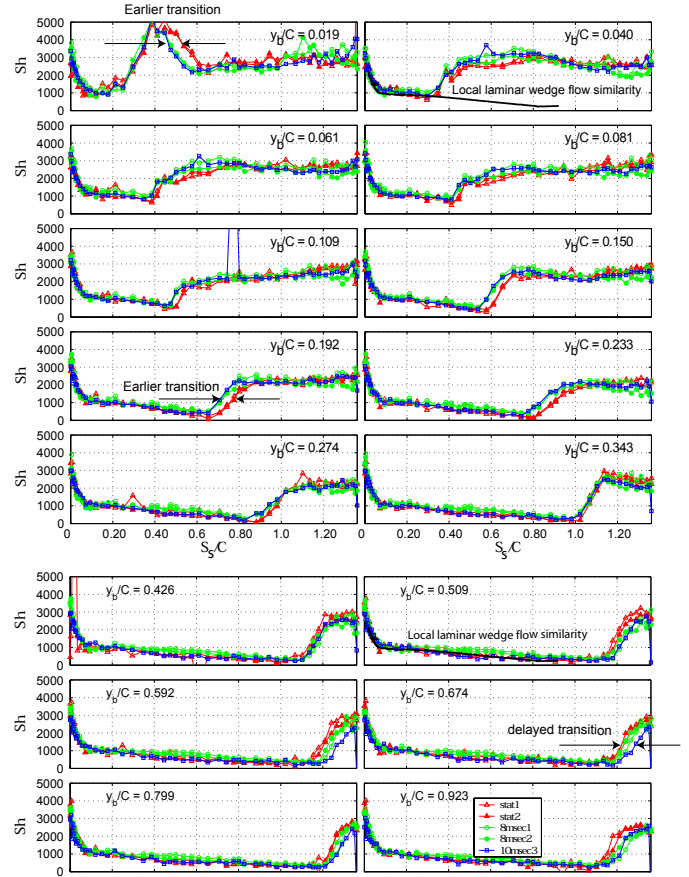


Figure 8. Experimental comparison of Sh on suction surface at various y_b/C ($0.019 < y_b/C < 0.923$)

For the stationary belt, the contour plot of the distribution of the Sherwood number (Sh) on the pressure surface of the blade is shown in Fig. 10(a). In this case, the trailing edge of the blade is located at $S_p/C = 1.07$. The leading edge represents a region of high mass transfer due to the direct impingement of the inlet flow. The pressure leg forms part of the passage vortex and has little influence on the overall mass transfer on the pressure surface. Between $0.45 < S_p/C < 1$, the waviness in Sh has been previously related [37] to the formation and development of Taylor-Gortler vortices. It was shown that the spanwise periodic variation in Sh was due to a series of counter-rotating vortex pairs, producing upwash and downwash fluid motion. Except for near the leading and trailing edges of the blade, a negligible difference between the numerical and the experimental results is observed in the mid-chord region of the blade ($0.2 < S_p/C < 0.8$) below y_b/C of 0.5.

For belt speeds of 8 and 10 m/sec , similar plots are shown in Figs.10(b) - 10(c). The formation of the Taylor-Gortler vortices is significant for $u_w = 8 \text{ m/sec}$. A detailed comparison of

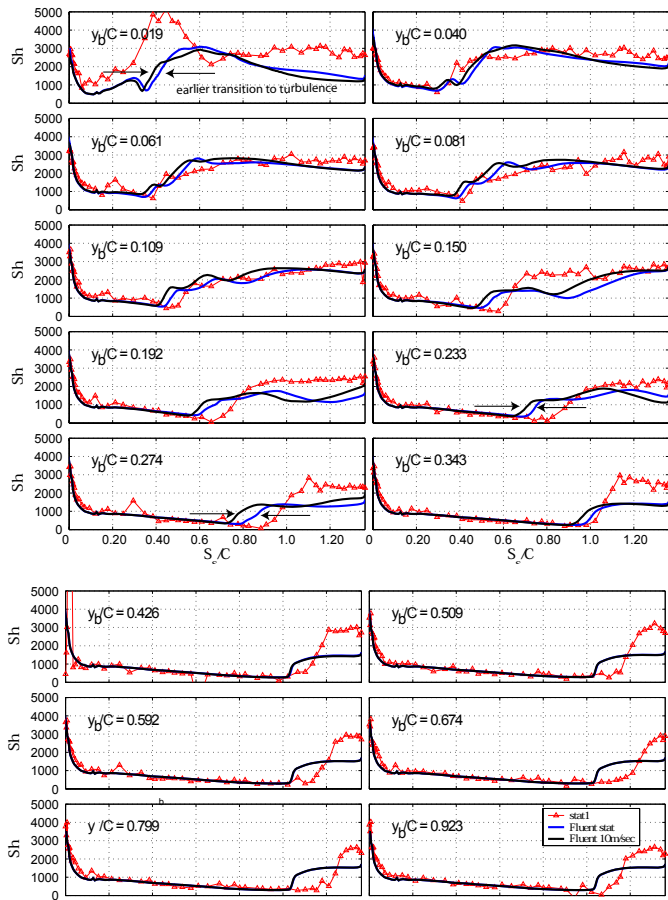


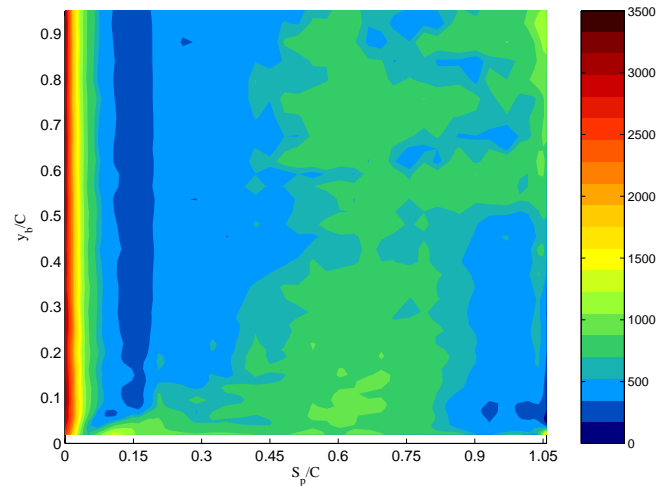
Figure 9. Comparison of CFD vs. experimental Sh on suction surface

the Sherwood number (Sh) at various span heights (y_b/C) for different belt-freestream velocity ratios (Fig. 11), shows a negligible effect of the inlet skew. In addition, the CFD model is in good prediction with the experimental results in the region $0.2 < S_p/C < 0.7$ (Fig. 12). In the near endwall region ($y_b/C < 0.09$) close to the leading edge of the blade ($S_p/C < 0.2$), the CFD results deviate from the experimental results probably due to the inability of the present turbulent model to predict the highly turning flow.

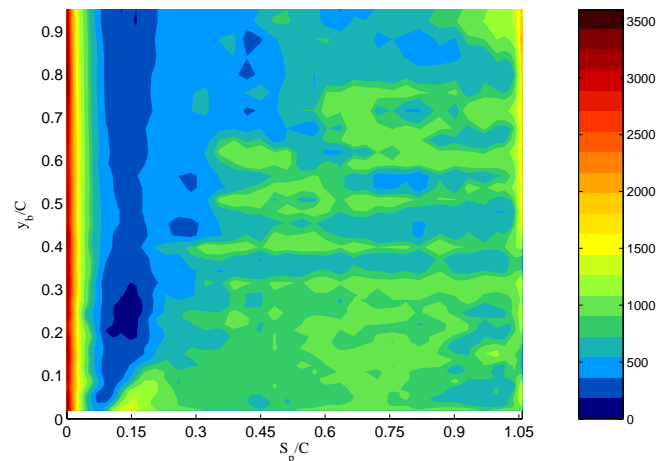
CONCLUSIONS

The effect of an inlet skew on the heat/mass transfer coefficients on a simulated gas-turbine blade is investigated in this study. The following conclusions can be drawn:

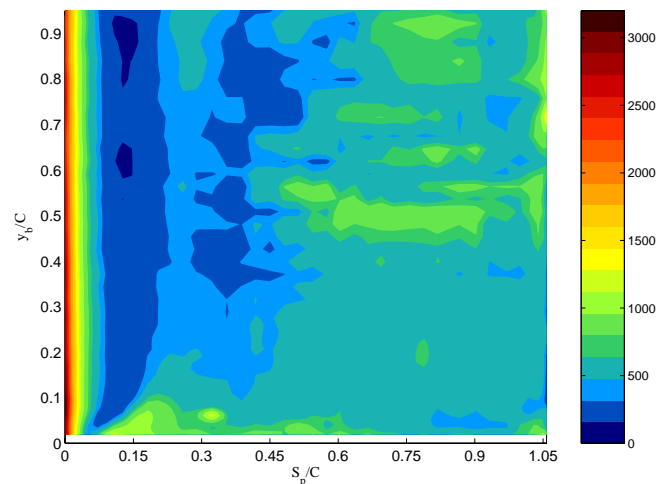
1. The velocity ratio (r) plays an important role in the variation of the heat/mass transfer coefficient on the suction surface. The suction side leg of the horseshoe vortex (V_{sh} , Fig. 1(a)) is strengthened and lifted by the inlet skew. This is evident



(a) Stationary belt



(b) $u_w = 8 \text{ m/sec}$



(c) $u_w = 10 \text{ m/sec}$

Figure 10. Experimental distribution of Sh on pressure surface

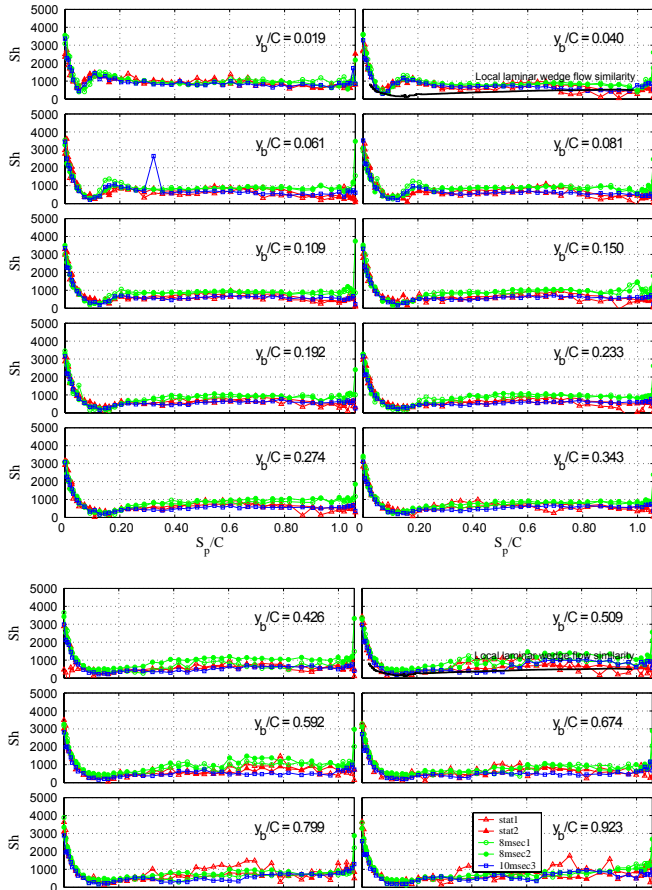


Figure 11. Experimental comparison of Sh on pressure surface at various y_b/C ($0.019 < y_b/C < 0.923$)

from an earlier transition to turbulence in the triangular region of Sh near the endwall (shown in Fig. 8). In addition, the negative skew delays transition in the two-dimensional region of the blade (Fig. 8).

- Surprisingly, the inlet skew has a negligible effect on the pressure surface. Since the pressure leg of the vortex is turned towards the companion suction surface, it does not affect the mass transfer on the pressure surface directly.

REFERENCES

- Wang, H., Olson, S., Goldstein, R., and Eckert, E., 1997. "Flow visualization in a linear turbine cascade of high performance turbine blades". *Journal of Turbomachinery*, **119**, p. 1.
- Carrick, H. B., 1977. "Secondary flow and losses in turbine cascades with inlet skew". In AGARD Conference Proceedings, no. 214, p. 9.
- Bindon, J., 1979. "Effect of hub inlet boundary layer skew-

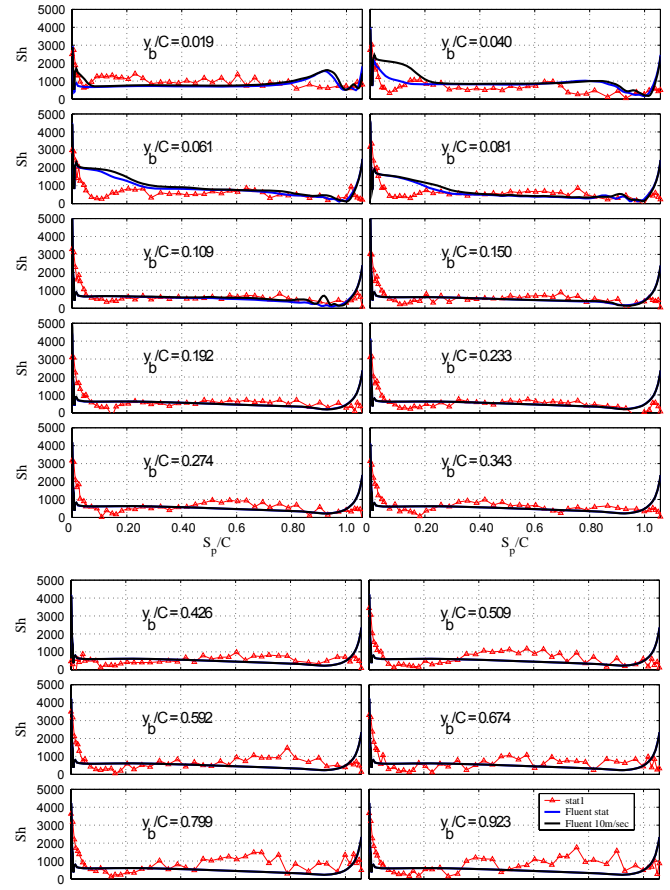


Figure 12. Comparison of CFD vs. experimental Sh on pressure surface

ing on the endwall shear flow in an annular turbine cascade". *ASME Paper*, **79-GT-13**.

- Bindon, J., 1980. "Exit plane and suction surface flows in an annular turbine cascade with a skewed inlet boundary layer". *International Journal of Heat and Fluid Flow*, **2**, p. 57.
- Walsh, J., and Gregory-Smith, D., 1990. "Inlet skew and the growth of secondary losses and vorticity in a turbine cascade". *Journal of Turbomachinery*, **112**, p. 633.
- Walsh, J., and Gregory-Smith, D., 1987. "Effect of inlet skew on the secondary flows and losses in a turbine cascade". *I Mech E Conference Publications (Institution of Mechanical Engineers)*, p. 15.
- Dullenkopf, K., Schulz, A., and Wittig, S., 1991. "The effect of incident wake conditions on the mean heat transfer of an airfoil". *Journal of Turbomachinery*, **113**(3), p. 412.
- Boletis, E., and Sieverding, C., 1991. "Experimental study of the three-dimensional flow field in a turbine stator preceded by a full stage". *Journal of Turbomachinery*, **113**(1), p. 1.

- [9] Zhang, L., and Han, J.-C., 1995. “Combined effect of free-stream turbulence and unsteady wake on heat transfer coefficients from a gas turbine blade”. *Journal of Heat Transfer*, **117**(2), p. 296.
- [10] Chaluvadi, V., Kalfas, A., Banieghbal, M., Hodson, H., and Denton, J., 2001. “Blade-row interaction in a high-pressure turbine”. *Journal of Propulsion and Power*, **17**(4), p. 892.
- [11] Schlienger, J., Kalfas, A., and Abhari, R., 2005. “Vortex-wake-blade interaction in a shrouded axial turbine”. *Journal of Turbomachinery*, **127**(4), p. 699.
- [12] Schobeiri, M., Ozturk, B., and Ashpis, D., 2005. “On the physics of flow separation along a low pressure turbine blade under unsteady flow conditions”. *Journal of Fluids Engineering, Trans ASME*, **127**(3), p. 503.
- [13] Schobeiri, M., Ozturk, B., and Ashpis, D., 2007. “Effect of reynolds number and periodic unsteady wake flow condition on boundary layer development, separation, and intermittency behavior along the suction surface of a low pressure turbine blade”. *Journal of Turbomachinery*, **129**(1), p. 92.
- [14] Allan, W., Ainsworth, R., and Thorpe, S., 2008. “Unsteady heat transfer measurements from transonic turbine blades at engine representative conditions in a transient facility”. *Journal of Engineering for Gas Turbines and Power*, **130**, p. 041901.
- [15] Olson, S., 1999. “Effects of high turbulence and wakes on mass transfer from gas turbine blades”. PhD thesis, University of Minnesota.
- [16] Srinivasan, V., and Goldstein, R., 2003. “Effect of endwall motion on blade tip heat transfer”. *Journal of Turbomachinery*, **125**(2), p. 267.
- [17] Ghosh, K., and Goldstein, R., 2009. “Effect of upstream shear on flow and heat (mass) transfer over a flat plate”. *ASME International Mechanical Engineering Congress and Exposition, Proceedings*, **10**, p. 519.
- [18] Han, S., 2004. “The heat and mass transfer analogy factor, nu/sh for 2-d and 3-d boundary layers”. PhD thesis, University of Minnesota.
- [19] Papa, M., 2006. “Influence of blade leading edge geometry and upstream blowing on the heat/mass transfer in a turbine cascade”. PhD thesis, University of Minnesota.
- [20] Schmidt, E., 1929. “Verdunstung und warmeuegang”. *Gesundheits-Ingenieur*, **29**, p. 525.
- [21] Nusselt, W., 1930. “Warmeuegang, diffusion und verdunstung”. *Math. Mechanik*, **2**, p. 105.
- [22] Goldstein, R., and Cho, H., 1995. “A review of mass transfer measurements using naphthalene sublimation”. *Experimental Thermal and Fluid Science*, **10**(4), p. 416.
- [23] Eckert, E., Sakamoto, H., and Simon, T., 2001. “The heat/mass transfer analogy factor, nu/sh , for boundary layers on turbine blade profiles”. *International Journal of Heat and Mass Transfer*, **44**, p. 1223.
- [24] Kline, S., and McClintock, F., 1953. “Describing uncertainties in single sample experiments”. *Mechanical Engineering*, **75**, p. 3.
- [25] Cho, K., 1989. “Measurement of the diffusion coefficient of naphthalene into air”. PhD thesis, State Univ. New York at Stony Brook.
- [26] Chen, P., and Wung, P., 1990. “Diffusion coefficient of naphthalene in air at room temperature”. *Personal Communication*.
- [27] Menter, F., 1994. “Two-equation eddy-viscosity turbulence models for engineering applications”. *AIAA Journal*, **32**, p. 1598.
- [28] Ameri, A., and Bunker, R., 2000. “Heat transfer and flow on the first-stage blade tip of a power generation gas turbine: Part 2-simulation results”. *Journal of Turbomachinery*, **122**(2), p. 272.
- [29] Garg, V., and Ameri, A., 2001. “Two-equation turbulence models for prediction of heat transfer on a transonic turbine blade”. *International Journal of Heat and Fluid Flow*, **22**, p. 593.
- [30] Shih, T.-P., and Lin, Y.-L., 2003. “Controlling secondary-flow structure by leading-edge airfoil fillet and inlet swirl to reduce aerodynamic loss and surface heat transfer”. *Journal of Turbomachinery*, **125**, p. 48.
- [31] Mumeric, F., Ljungkruna, L., and Sunden, B., 2006. “Numerical simulations of heat transfer and fluid flow for a rotating high-pressure turbine”. *Proceedings of the ASME Turbo Expo 2006 - Power for Land, Sea, and Air*, **6**, p. 1149.
- [32] Papa, M., Goldstein, R., and Gori, F., 2007. “Numerical heat transfer predictions and mass/heat transfer measurements in a linear turbine cascade”. *Applied Thermal Engineering*, **27**(4), p. 771.
- [33] Goldstein, R., Wang, H., and Jabbari, M., 1995. “The influence of secondary flows near the endwall and boundary layer disturbance on convective transport from a turbine blade”. *Journal of Turbomachinery*, **117**, p. 657.
- [34] Sparrow, E., Quack, H., and Boerner, C., 1970. “Local non-similarity boundary-layer solutions”. *AIAA Journal*, **8**, p. 1936.
- [35] Sonoda, T., 1985. “Experimental investigation on special development of streamwise vortices in a turbine inlet guide vane cascade”. *85-GT-20*.
- [36] Doorly, D., and Oldfield, M., 1985. “Simulation of wake passing in a stationary turbine rotor cascade”. *Journal of Propulsion and Power*, **1**, p. 316.
- [37] Wang, H., Olson, S., and Goldstein, R., 2005. “Development of taylor-gortler vortices over the pressure surface of a turbine blade”. *Journal of Heat Transfer*, **127**(5), p. 540.